PLOS COMPUTATIONAL BIOLOGY

RESEARCH ARTICLE

# Modeling suggests that virion production cycles within individual cells is key to understanding acute hepatitis B virus infection kinetics

**Atesmachew Hailegiorgis[1☯], Yuji Ishida[2,3☯], Nicholson Collier[4,5], Michio Imamura[3], Zhenzhen Shi[1], Vladimir Reinharz[6], Masataka Tsuge[1,3,7], Danny Barash[8], Nobuhiko Hiraga[3], Hiroshi Yokomichi[2], Chise Tateno[2,3], Jonathan Ozik[4,5], Susan L. Uprichard[1,9], Kazuaki Chayama[3,10,11,12]*, Harel Dahari[1]***

**1** The Program for Experimental & Theoretical Modeling, Division of Hepatology, Department of Medicine, Stritch School of Medicine, Loyola University Chicago, Maywood, Illinois, United States of America, **2** PhoenixBio Co., Ltd., Hiroshima, Japan, **3** Research Center for Hepatology and Gastroenterology, Graduate School of Biomedical and Health Sciences, Hiroshima University, Hiroshima, Japan, **4** Consortium for Advanced Science and Engineering, University of Chicago, Chicago, Illinois, United States of America, **5** Decision and Infrastructure Sciences, Argonne National Laboratory, Argonne, Illinois, United States of America, **6** Department of Computer Science, Université du Québec à Montréal, Montreal, Canada, **7** Department of Gastroenterology, Graduate School of Biomedical & Health Sciences, Hiroshima University, Hiroshima, Japan, **8** Department of Computer Science, Ben-Gurion University, Beer-Sheva, Israel, **9** The Infectious Disease and Immunology Research Institute, Stritch School of Medicine, Loyola University Chicago, Maywood, Illinois, United States of America, **10** RIKEN Center for Integrative Medical Sciences, Yokohama, Japan, **11** Collaborative Research Laboratory of Medical Innovation, Graduate School of Biomedical and Health Sciences, Hiroshima University, Hiroshima, Japan, **12** Hiroshima Institute of Life Sciences, Hiroshima, Japan

☯ These authors contributed equally to this work.
* chayama@hiroshima-u.ac.jp (KC); hdahari@luc.edu (HD)

## Abstract

Hepatitis B virus (HBV) infection kinetics in immunodeficient mice reconstituted with humanized livers from inoculation to steady state is highly dynamic despite the absence of an adaptive immune response. To recapitulate the multiphasic viral kinetic patterns, we developed an agent-based model that includes intracellular virion production cycles reflecting the cyclic nature of each individual virus lifecycle. The model fits the data well predicting an increase in production cycles initially starting with a long production cycle of 1 virion per 20 hours that gradually reaches 1 virion per hour after approximately 3–4 days before virion production increases dramatically to reach to a steady state rate of 4 virions per hour per cell. Together, modeling suggests that it is the cyclic nature of the virus lifecycle combined with an initial slow but increasing rate of HBV production from each cell that plays a role in generating the observed multiphasic HBV kinetic patterns in humanized mice.

OPEN ACCESS

**Citation:** Hailegiorgis A, Ishida Y, Collier N, Imamura M, Shi Z, Reinharz V, et al. (2023) Modeling suggests that virion production cycles within individual cells is key to understanding acute hepatitis B virus infection kinetics. PLoS Comput Biol 19(8): e1011309. https://doi.org/10.1371/journal.pcbi.1011309

**Editor:** Eric Lofgren, Washington State University, UNITED STATES

**Received:** November 2, 2022

**Accepted:** June 26, 2023

**Published:** August 3, 2023



**Data Availability Statement:** The experimental data is provided in Table A in S1 Text. The agent-based modeling code is available on GitHub (https://github.com/szztracy/ModelingHBVKineticsInMice). We provide a link to run the agent-based model from a web browser: https://cloud.anylogic.com/model/9e9b5f21-01c0-41a7-8b6b-793808d1c6ea?mode=SETTINGS.

**Funding:** This work was supported by funding of the United States National Institutes of Allergy and

Infectious Diseases (Grant numbers R01AI144112 to SLU and HD and R01AI146917 to HD), the Japan Agency for Medical Research and Development (AMED grant 19fk0210020h0003 to KC), the Promotion of Joint International Research (Fostering Joint International Research) from Japan Society for the Promotion of Science (Grant number: 17KK0194 to KC). The funders had no role in study design, data collection and analysis, decision to publish, or preparation of the manuscript.

**Competing interests:** I have read the journal's policy and the authors of this manuscript have the following competing interests: YI, HI and CT are Phoenix Bio employees.

## Author summary

A surprisingly complex hepatitis B virus (HBV) infection kinetics was observed in chimeric urokinase type plasminogen activator transgenic, severe combined immunodeficient (uPA-SCID) mice with humanized livers. Here we developed an agent-based model (ABM) to reproduce the observed multiphasic HBV dynamics. To model the fundamental cyclic dynamics of viral infections (i.e., the underlying viral lifecycle), capture the inherent asynchronous nature of viral infections, and mimic the amplification of these successive virion release cycles from individual cells, our newly developed ABM approach enables conceptualization of discrete virus production as cycles allowing for accurate recapitulation of the complex kinetic pattern observed in vivo and providing new theoretical frontiers to understanding viral dynamics.

## Introduction

Despite the availability of an effective vaccine for the prevention of hepatitis B virus (HBV), HBV infection continues to impose an enormous burden with an estimated of 270 million chronically infected individuals and about 1 million deaths every year due to complications of HBV, including cirrhosis and liver cancer [1]. Research to elucidate the molecular mechanisms that regulate the HBV lifecycle and infection outcome (i.e., clearance vs. persistence) has been hampered by the lack of model systems that recapitulate HBV infection [2]. Significant attempts have been made to develop small animal models of HBV infection [3]. The most successful small animal HBV infection model approach is based on liver-repopulation in immunodeficient mice repopulated with primary human hepatocytes as these are the natural target of HBV [4–8].

We previously assessed acute HBV infection kinetics from infection initiation to viral steady state in 42 chimeric urokinase-type plasminogen activator transgenic/severe combined immunodeficient (uPA-SCID) mice reconstituted with human hepatocytes [9]. Serum HBV DNA was measured at varying intervals starting as early as 1 min post-inoculation and going out 63 days [9]. Despite varying HBV doses ($10^4$–$10^8$ genome equivalents) and different batches of human hepatocytes, a consistent pattern of distinct phases was observed [9] (Fig 1). To elucidate the processes that result in the complex HBV kinetics observed from initiation to steady state in these mice, we have developed an agent-based modeling (ABM) approach that considers the cyclic nature of the viral lifecycle within individual cells and the resulting distinct waves of viral release and spread. Specifically, the incorporation of viral production cycles within individual infected cells starting with an initially slow production (1 virion every 20 hours) that increases over time to reach steady state of 4 virions every hour recapitulates the multiphasic kinetic patterns. Using ABM to more accurate conceptualize HBV production as cycles rather than a continuous increase thus allows us to reproduce the observed HBV infection dynamics in vivo and provides a new modeling approach for simulating viral dynamics during acute infection.

## Results

### Agent-based modeling of HBV dynamics

While we showed [9] that the standard experimental approach of measuring HBV DNA levels in serial serum samples from infected mice allows for the calculation of average viral parameters and demonstrates complex multiphasic pattern of viral amplification from inoculation to

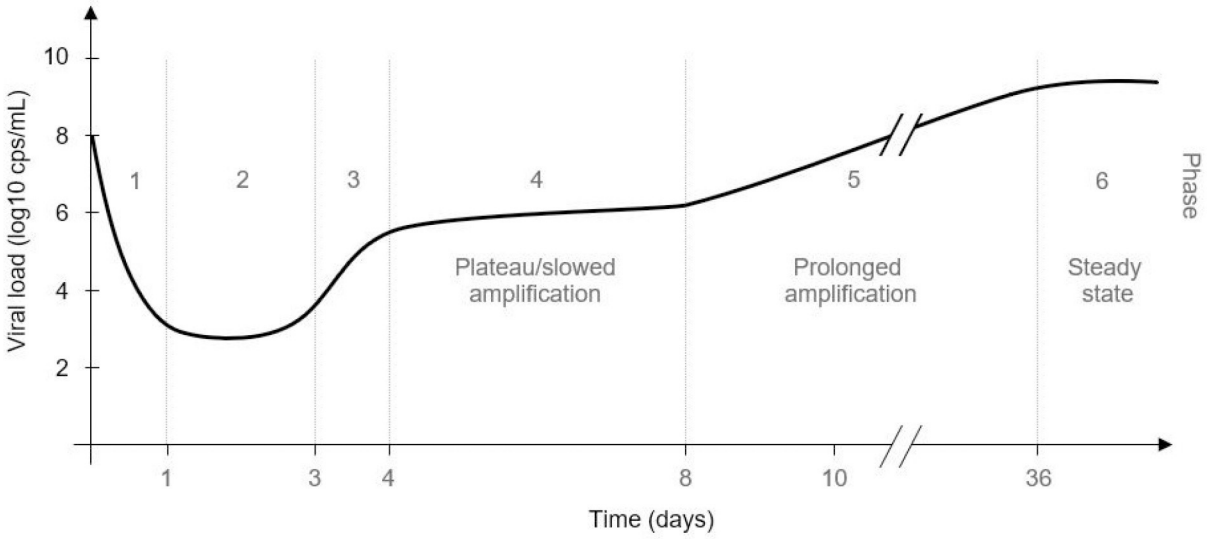


**Fig 1. Overview of the main HBV kinetic patterns determined based on analysis of 42 humanized mice from inoculation to steady state.** HBV kinetic phases from mice after inoculation with $10^8$ copies HBV DNA: Phase 1, rapid decline; Phase 2, lower viral plateau; Phase 3, rapid increase; Phase 4, extremely slow increase or plateau; Phase 5, prolonged amplification; Phase 6, steady state. Modified from (9); two initial clearance phases have been combined into one, now jointly termed Phase 1.

https://doi.org/10.1371/journal.pcbi.1011309.g001

steady state (Fig 1), it masks the asynchronous infection of individual cells as the virus spreads [10]. We developed an ABM to investigate the dynamics underlying the observed multiphasic HBV kinetic pattern in humanized mice. The ABM accounts for two types of agents: human hepatocytes (cells) and virus in blood (Fig 2A). The cell agents, which are characterized by their infection stage are represented by a square lattice of $3\times10^8$ cells i.e., the estimated number of human hepatocytes in the humanized mice [11]. The cell agents can be in one of the following three discrete states: uninfected susceptible target (T), infected cell in eclipse phase ($I_E$) (i.e., not yet releasing progeny virus), or productively infected cell secreting progeny virus ($I_P$). Due to the absence of an adaptive immune response in these mice, cell death is not considered in the model, hence the cell number was kept constant throughout the simulation period. The virus agent, V, represents the amount of HBV in the blood and is characterized in the ABM as a single global agent which may infect susceptible target cells with rate constant $\beta$ to become infected cells in eclipse phase ($I_E$) or to be cleared from blood with rate constant $c$ (Fig 2A). The ABM execution is an iterative process where each iteration represents a "tick" or a discrete time step, where 1 step = 1 hour.

Because HBV is a noncytolytic virus [12] intracellular viral production increases over time until reaching a resource restriction plateau. To model this on a per cell basis, we quantify both the amount of viral production by infected cells at a given time and the production cycle, i.e., the time interval over which the cell produces virus (Fig 2B). To capture such dynamics, we formulated the following equations.

The amount of virion produced, P, at production cycle $\tau$ is determined as:

$$P(\tau) = \frac{P_{st}}{1 + e^{-(\tau-\alpha)}} \quad (1)$$

where, $P(\tau)$ is number of virions produced by infected cells a $\tau$, $P_{st}$ is steady state virus production, $\alpha$ is number of cycles to reach to 50% of $P_{st}$, $\gamma$ is steepness of the production curve, and $\tau$ is the production cycle. Viral production, $P_{st}$, is estimated at steady state when all target cells

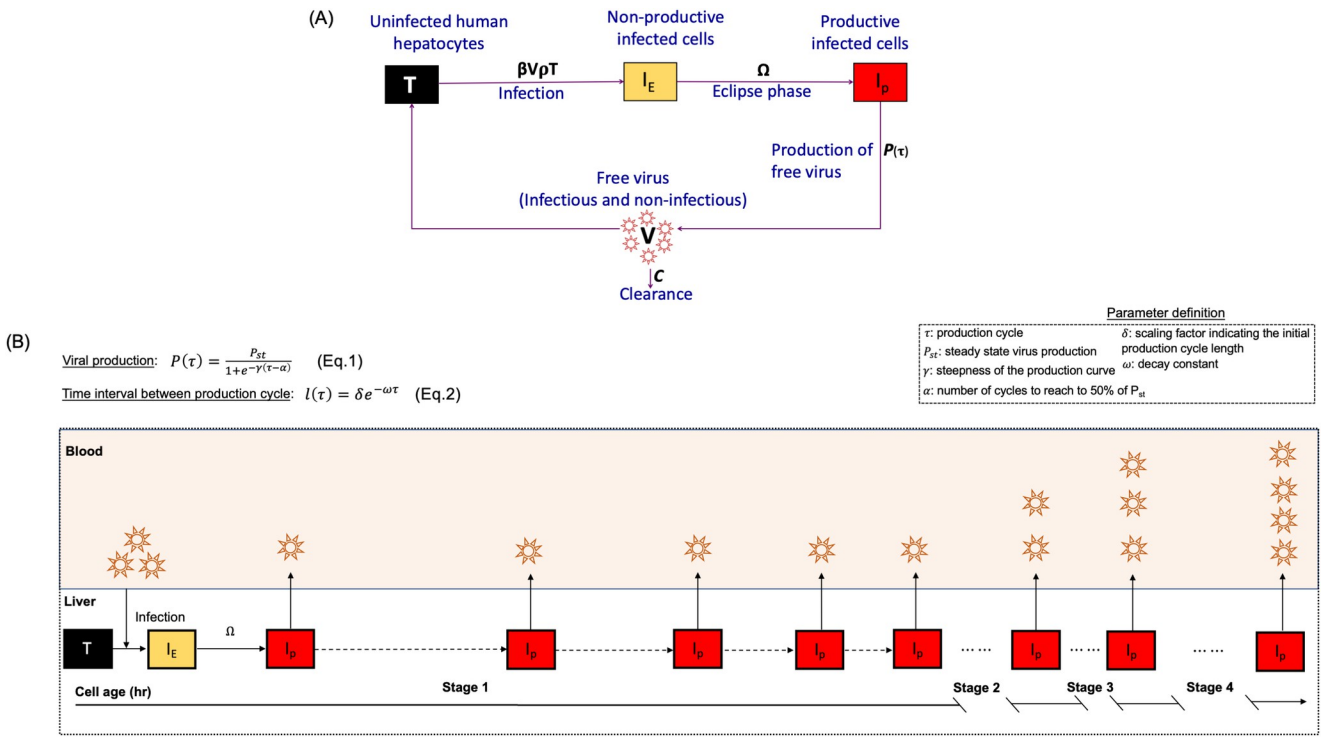


**Fig 2. Schematic diagram of the ABM. (A)** The human hepatocytes can be only in one of the following three phases at a given time; T = uninfected cells which are termed as target or susceptible cells, $I_E$ = HBV-Infected cells in eclipse phase (i.e., not yet releasing virions), $I_P$ = productively HBV-infected cells (i.e., actively releasing virions). The free virus in blood, V, is composed of infectious and non-infections virions. The parameter ρ represents the fraction of virions that are infectious, β represents the infection rate constant, Ω represents eclipse phase duration, c, represents viral clearance from blood and $P(\tau)$ (Eq 1) represents virion secretion from $I_P$. **(B)** Schematic diagram of viral production cycle for an individual infected human hepatocyte. P(τ) is the number of virions produced by an infected cell, and $l(\tau)$) is the time interval between production cycle (h). The virions were initially released by $I_P$ starting with a long production cycle of 1 virion per cell (Stage 1: ~0–2.5 days) that gradually reaches a production of 2 virions per cell with a shorten production cycle (Stage 2: ~2.5–3 days) and then proceeds to 3 virions per cell (Stage 3: ~3–4 days) before virion production increases to reach to a steady state production rate of 4 virions per hour per cell (Stage 4: ~ 4 days onwards).

https://doi.org/10.1371/journal.pcbi.1011309.g002

are infected, therefore $P_{st} = cV_{st}/I_p$ where $V_{st}$ represents viral load at steady state, and $c$ represents the virus clearance rate constant from blood.

And the interval between cycles is determine by an exponential decay function with:

$$l_\tau = \delta e^{-\omega\tau} \quad (2)$$

Where $l_\tau$ is interval between production cycle, $\tau$ is the production cycle, $\delta$ is scaling factor indicating the initial production cycle length, and $\omega$ is decay constant. In the model, both P(τ) and $l_\tau$ are roundup to the nearest integer. The combination of Eqs 1 and 2 allows for each productively infected cell to slowly produce virions once $I_E$ becomes $I_P$ with increasing numbers of secreted virions within shorter time intervals until the cell reaches a steady state production.

## ABM reproduces multiphasic HBV kinetics after a high dose viral inoculation

The model reproduces well the complex HBV DNA serum patterns observed in 4 mice (Table A in S1 Text) inoculated with $10^8$ HBV genome equivalents and followed from inoculation until day 51 post-inoculation (p.i.) (Fig 3 and Figs A-D in S1 Text). The estimated model parameters based on best fit for the 4 mice (M1 -M4) are shown in Table 1. A graph showing the in silico kinetics of the changing human hepatocyte (cell) states (Fig 4A) and representative

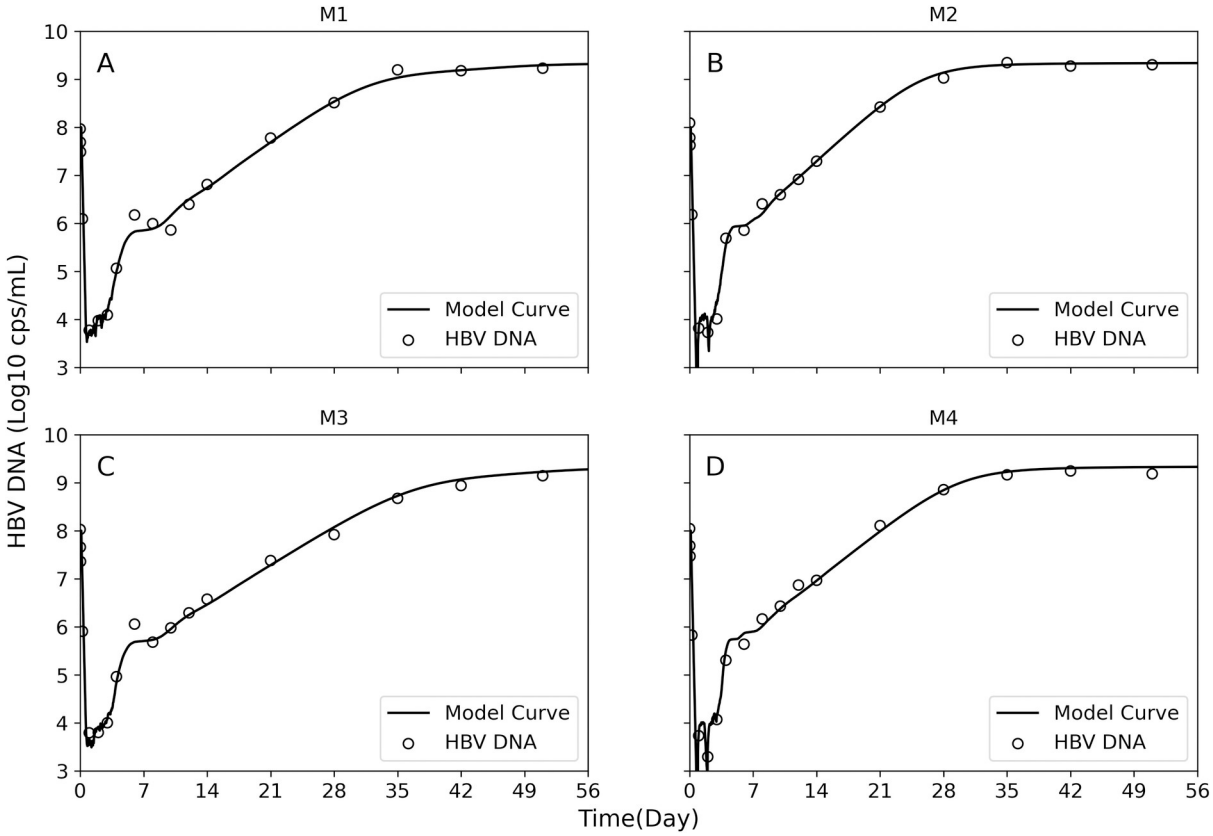


**Fig 3.** Model best fit (solid curves) with measured HBV DNA kinetics in blood (circles) in four mice M1 **(A)**, M2 **(B)**, M3 **(C)** and M4 **(D)** inoculated with $10^8$ HBV genome equivalents. Estimated parameters are shown in Table 1.

https://doi.org/10.1371/journal.pcbi.1011309.g003

pictures of the cell populations at distinct time points (Fig 4B) during the simulation of infection for mouse 1 (M1) reveals that while serum HBV DNA is multiphasic (Fig 3), the total cell-state kinetics are simple, e.g., uninfected productively infected cells follow simple sigmoidal-like patterns (Fig 4A, green and red curves).

## Virus parameter estimates of individual cells that allow for simulation of the observed complex serum viral patterns

The model provides insights into early virus-host dynamics of individual cells from infection initiation to steady state that unmask the nature of the observed complex serum viral kinetic patterns. To fit the data, the model predicts a variable eclipse phase ranging from 5–50 hours in the 4 mice inoculated with $10^8$ HBV genome equivalents (Table 1). Using M1 as a representative example, the simulated virion production with two eclipse phase durations of 9 hr (Fig 5A, shaded box) and 48 hr (Fig 5C, shaded box) illustrates the delay in virion production that results from the longer eclipse phase without affecting subsequent virus production cycles. Post-eclipse phase, the model predicts viral release from productively infected cells starts slowly with a long production cycle of 1 virion per 20 hours that gradually reaches 1 virion per hour (Fig 5B and 5D) after ~3–4 days before virion production increases to reach to a steady state production rate of 4 virions per hour per cell (Fig 5A and 5C). A similar picture was found for mice M2, M3 and M4 (Fig V in S1 Text).

**Table 1. Best estimated ABM parameters for calibrated mice and their estimated space (J<0.7).** Parameters are defined in Eqs 1 and 2; GE, genome equivalent; J-score, represents the objective function (Eq 3) score of the genetic algorithm (GA) fits where the min J-score is the best fit curves shown in Figs 3 and 7. Parameter estimates shown in () represent the min and max of all GA fits with J-score < 0.7 shown in Figs A-G in S1 Text with their statistics in Table C in S1 Text. Parameter pair plots and their correlation plots are shown in Figs H-N in S1 Text and Figs O-U in S1 Text, respectively.

| Mouse # | Initial viral input [GE/ml] | Eclipse phase [hr] ($\Omega$) | Virus production at steady state, [GE/ml] ($P_{st}$) | Steepness of the production curve [$hr^{-1}$] ($\gamma$) | Number of cycles to reach 50% of $P_{st}$ [hr] ($\alpha$) | Initial production cycle length [hr] ($\delta$) | Decay constant [$hr^{-1}$] ($\omega$) | Infection rate ($\beta$) | J-Score [Min-Max] | % of J<0.70 [# of simulations] |
|---|---|---|---|---|---|---|---|---|---|---|
| M1 | $10^8$ | 9–48 (5–50) | 4 (2–5) | 0.1 (0.1–0.9) | 20 (10–29) | 26 (18–30) | 0.51 (0.33–0.84) | 0.019 (0.01–0.04) | 0.29–0.70 | 80% [1500] |
| M2 | $10^8$ | 15–40 (7–50) | 4 (2–5) | 0.62 (0.1–0.9) | 15 (14–30) | 30 (15–30) | 0.80 (0.30–0.90) | 0.024 (0.01–0.084) | 0.24–0.70 | 81% [1500] |
| M3 | $10^8$ | 7–48 (5–50) | 4 (2–4) | 0.1 (0.1–0.9) | 14 (10–30) | 23 (15–30) | 0.40 (0.30–0.90) | 0.013 (0.01–0.04) | 0.28–0.70 | 79% [1500] |
| M4 | $10^8$ | 15–33 (6–46) | 4 (2–5) | 0.88 (0.1–0.9) | 10 (10–30) | 26 (21–30) | 0.57 (0.30–0.81) | 0.015 (0.01–0.069) | 0.25–0.70 | 82% [1500] |
| M5 | $10^7$ | 17–18 (12–21) | 4 (4) | 0.22 (0.16–0.32) | 30 (25–30) | 26 (26) | 0.50 (0.45–0.57) | 0.038 (0.030–0.045) | 0.59–0.70 | 45% [1500] |
| M6 | $10^6$ | 10–26 (5–50) | 4 (4) | 0.58 (0.1–0.9) | 18 (10–30) | 29 (15–30) | 0.66 (0.33–0.99) | 0.026 (0.01–0.20) | 0.27–0.70 | 91% [1500] |
| M7 | $10^4$ | 36–50 (5–50) | 2 (2–3) | 0.73 (0.1–0.9) | 29 (11–30) | 30 (15–30) | 0.60 (0.3–0.85) | 0.016 (0.01–0.04) | 0.47–0.70 | 82% [1500] |

https://doi.org/10.1371/journal.pcbi.1011309.t001

## Dissecting the nature of each serum HBV DNA kinetic phase

Focusing on the details of the model simulation for representative M1, the estimated serum HBV DNA is shown on a time scale that allows visualization of each serum HBV DNA kinetic phase (Fig 6A and 6B). The number of non-productive ($I_E$) and productive ($I_P$) infected cells along with the average virion production per productive cells are plotted on the same scale for direct comparison (Fig 6C and 6D).

During the first 6 hours p.i. (Fig 6A, Phase 1), as the model recapitulates the rapid serum HBV DNA (V) clearance from the blood ($t_{1/2}$ = 1 hr), it predicts that about $1\times10^5$ cells were infected, i.e., the first wave of infection. This consists of an initial peak of eclipse phase cells ($I_E$) (Fig 6C, solid gold line).

As the $I_E$ cells gradually transition into $I_P$ cells (Fig 6C, solid red line) the resulting low initial virion production (Fig 6C, green line), balances continual viral clearance resulting in the lower serum viral plateau (Fig 6A, Phase 2).

The first rapid increase in HBV serum levels (Fig 6A, Phase 3) occurs once the virus production rate increases in the initially infected $I_P$ cells (Fig 6C, green line). During Phase 3 the number of $I_P$ cells remains constant (Fig 6C, solid red line) while the second wave of newly infected $I_E$ cells start to emerge (Fig 6C, solid gold line).

The observed intermediary serum HBV DNA steady state (or plateau) is recapitulated by the model (Fig 6A, Phase 4) as the majority of $I_P$ cells are at steady state levels of viral production and the new increasing numbers of $I_P$ cells are in the early low level virus production phase of infection (Fig 6C, increasing solid red line). Likewise, the increasing number of $I_E$ cells do not contribute to virion production (Fig 6C, increasing solid gold line) resulting in an overall decrease in the per cell virion production rate (Fig 6C, decreasing green line).

As the infection becomes less synchronized due to the stochasticity that exists in the timing of individual infection events and target cells become limiting, the distinct cycles of infection become less discernable and all subsequent amplification appears as a single viral exponential

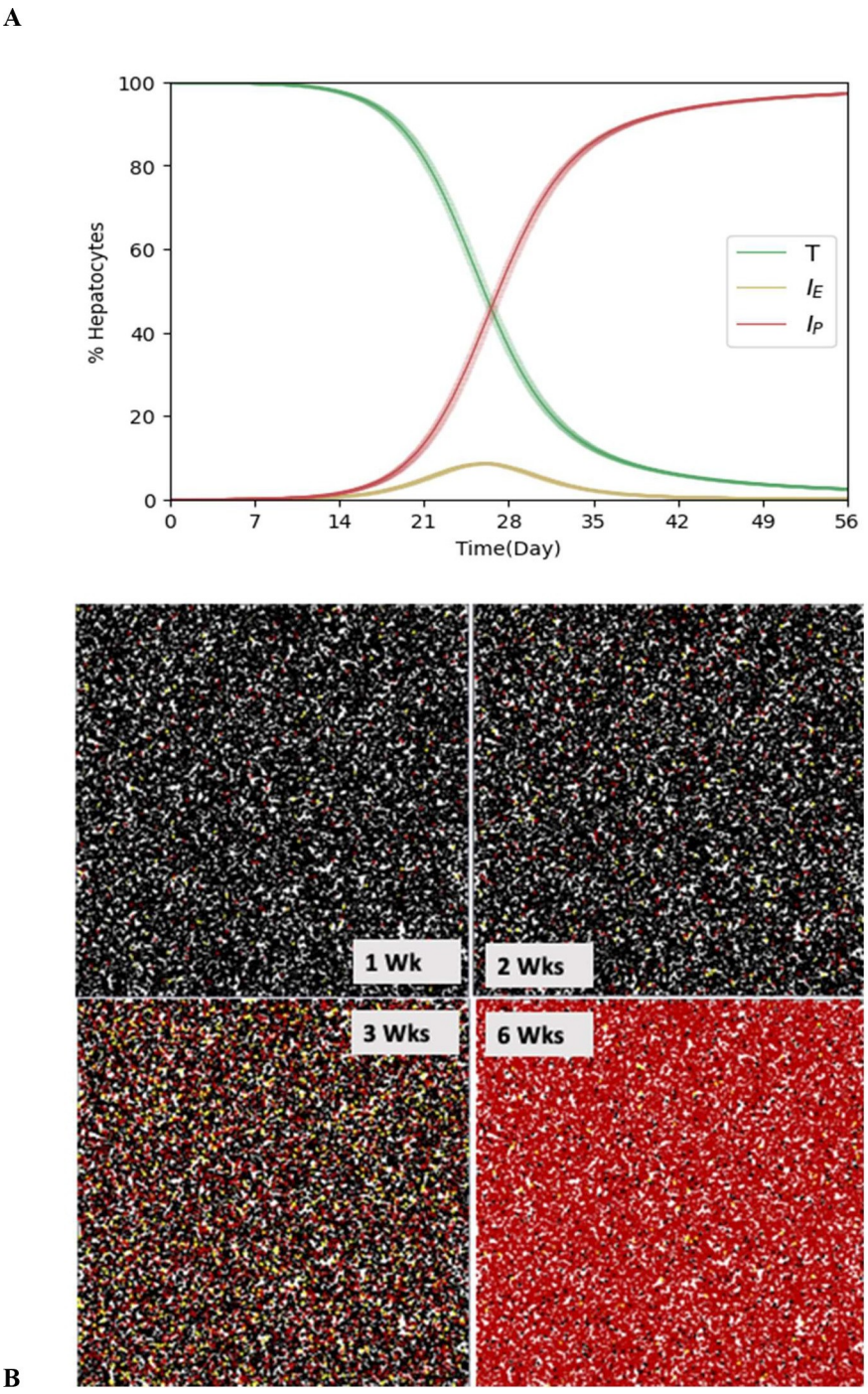


**Fig 4. Simulated human hepatocytes infection kinetics post simulated inoculation.** (**A**) Uninfected cells (T, black line), Infected non-productive cells ($I_E$, yellow line), and productively infected cells ($I_P$, red line) kinetics. The bold lines of each simulation curve represent the average of 1,000 independent runs with different random seeds and the shaded areas denote 95% confidence interval of those 1,000 runs. (**B**) Cell states observed from a representative run in the 2D lattice at 1, 2, 3, and 6 weeks post simulated inoculation. Uninfected cells (T, black cells), Infected non-productive cells ($I_E$, yellow cells), and productively infected cells ($I_P$, red cells). The ABM results shown represent the best fit of mouse M1 (Fig 3A and Table 1). The spatial structure on the 2D lattice was not considered in the ABM to affect viral infection spread.

https://doi.org/10.1371/journal.pcbi.1011309.g004

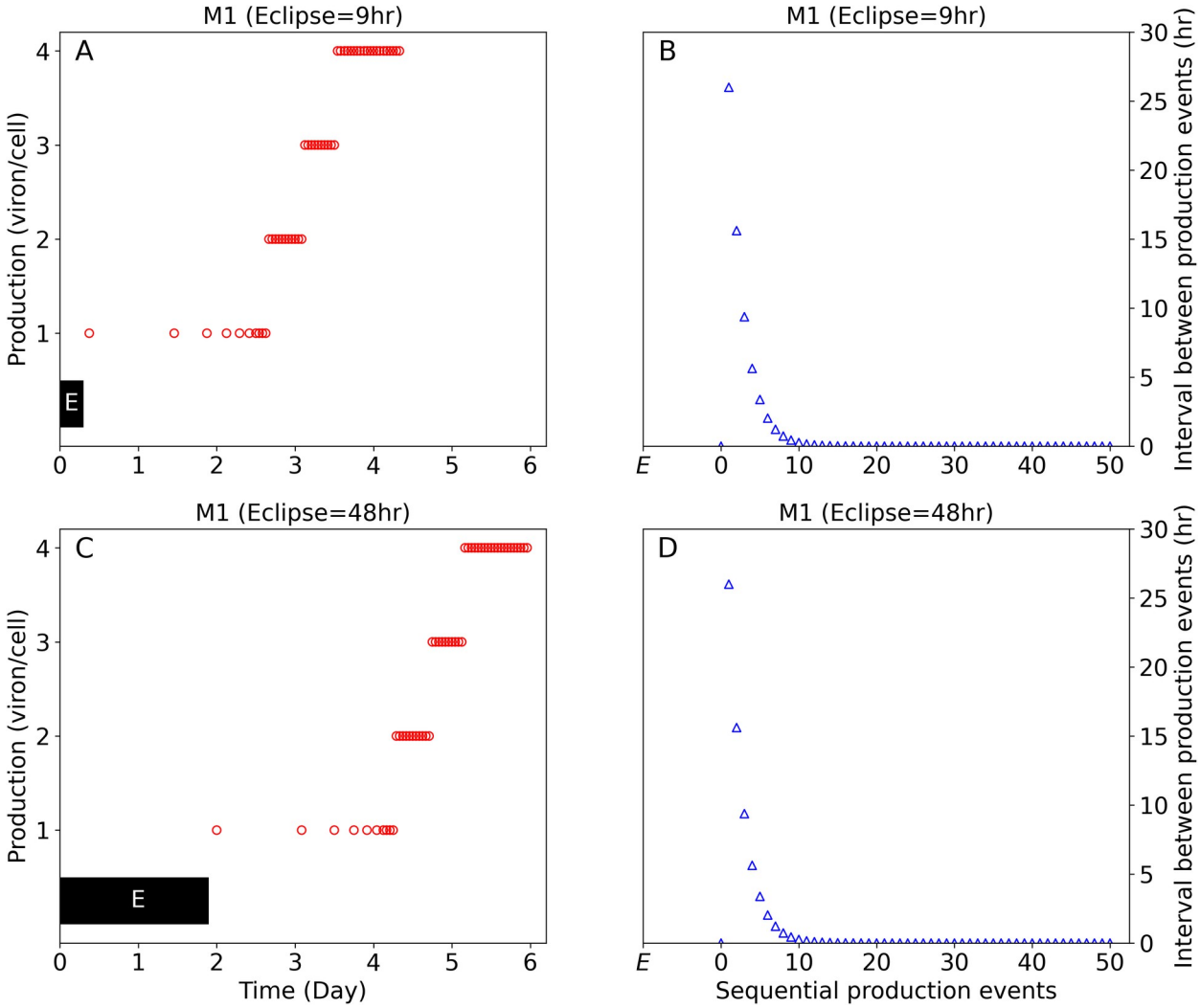


**Fig 5.** HBV virion production (circles) and viral production cycles (triangles) in representative mouse (M1) inoculated with $10^8$ HBV genome equivalents shown in Fig 3A. (**A** and **B**) represent infected cells with minimum eclipse phase of 9 hr (black-shaded "E"). (**C** and **D**) infected cells with maximum eclipse phase of 48hr. Similar predictions for mice M2, M3 and M4 are shown in Fig V in S1 Text.

https://doi.org/10.1371/journal.pcbi.1011309.g005

expansion from day ~8 until ~30 days p.i. (Fig 6B, Phase 5) during which the final target cells are infected and become productive (Fig 6D, solid gold and red lines, respectively) and subsequently progress towards maximal average viral production (Fig 6D, green line).

Once all the target cells are productively infected (Fig 6B, solid red line) and achieve maximal average viral production (Fig 6D, green line), serum HBV levels attained steady state (Fig 6B, Phase 6).

## ABM reproduces multiphasic HBV kinetics after low dose infection

We previously showed that lower inoculation of $10^7$, $10^6$ and $10^4$ HBV genome equivalents in humanized uPA-SCID mice led to a delayed, but similar complex HBV kinetic pattern [9]. Therefore, we validated the model against this kinetic data (Table A in S1 Text) by changing only the inoculation dose in the model simulation. Importantly, the model reproduced well the kinetic patterns within the same parameter space estimated for mice that were inoculated with $10^8$ HBV genome equivalents (Fig 7, and Figs E-G in S1 Text and Table 1).

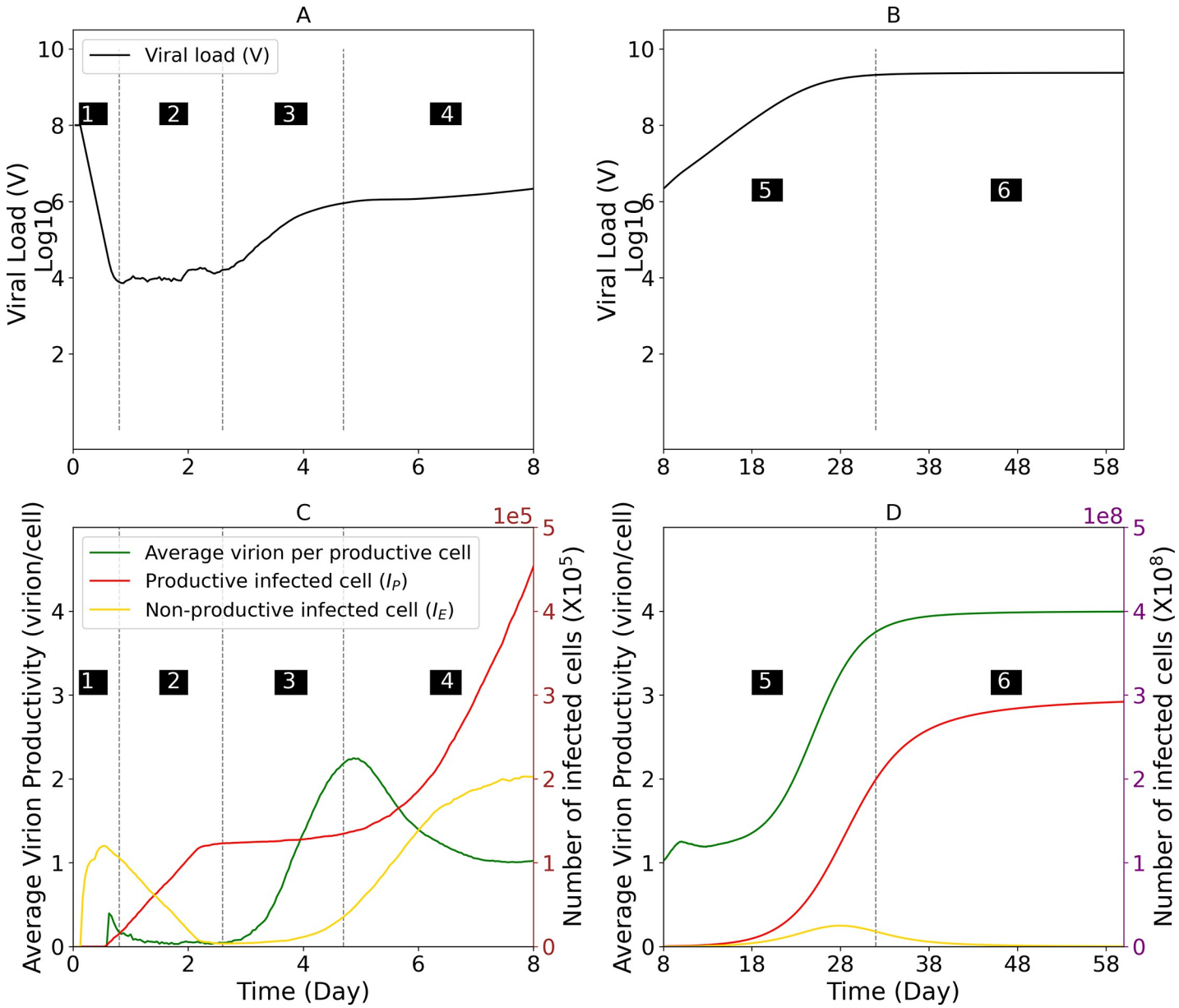


**Fig 6. Model parameter estimates for representative mouse M1.** (**A and B**) Simulated serum viral load. (**C and D**) The number of total cells in eclipse phase (solid gold line), productively infected cells (solid red line) and the average virion production (or secretion) per productively infected cells (solid green line) per time post inoculation. Graphs are divided according to the kinetic phases of HBV serum DNA amplification observed experimentally in Fig 1. Phases 5 and 6 are graphed separately to accommodate the larger y-axis scale required later in infection. Dashed vertical lines and black-shaded numbers indicating kinetic Phases 1–4 in (**A**) and (**C**) and Phases 5 and 6 in (**B**) and (**D**).

https://doi.org/10.1371/journal.pcbi.1011309.g006

## Short virion production cycle and eclipse phase lengths diminish multiphasic kinetic pattern

Having validated the ability of the model to accurately recapitulate the kinetics of HBV infection, we proceed to investigate how the two key features of the model, namely cellular eclipse phase and/or production cycle, might affect acute viral infection kinetics in general. To test the effect of shortening and/or lengthening the cellular eclipse phase and/or production cycle, in

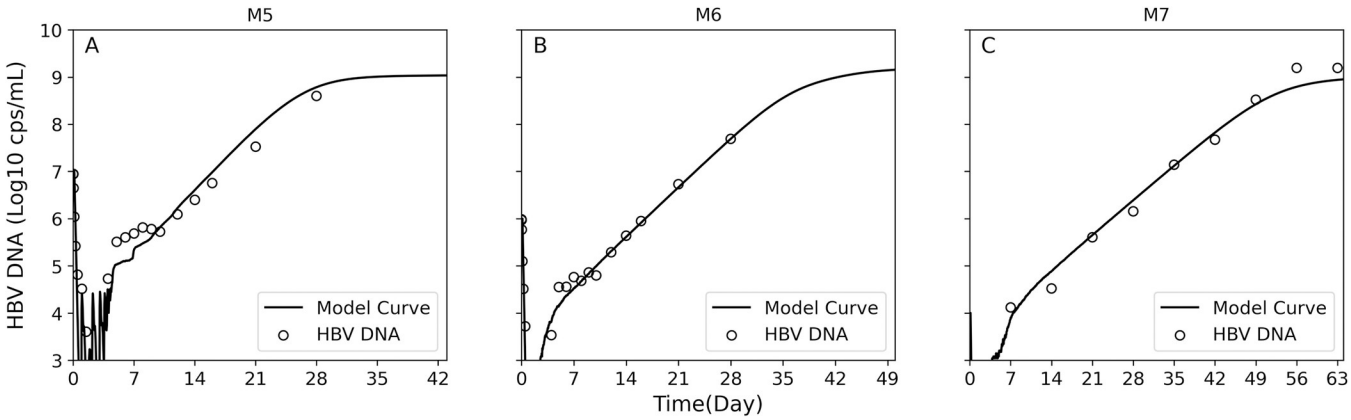


**Fig 7. Model validation.** Model best fit curves (solid lines) with measured HBV DNA kinetics (circles) in representative mice M5, M6 and M7 inoculated with and $10^7$ **(A)**, $10^6$ **(B)**, and $10^4$ **(C)** HBV genome equivalents, respectively. Estimated model parameters are shown in Table 1.

https://doi.org/10.1371/journal.pcbi.1011309.g007

silico simulations were performed using HBV viral parameters estimated for mouse 1 (M1) as a reference for 14 days (Fig 8) and 56 days (Fig W in S1 Text) post-inoculation.

Lengthening the cellular eclipse phase resulted in an initial period of no viral production followed by a delayed but multiphasic viral amplification (Phases 2–6) (Fig 8A, red dotted line). In contrast, a short eclipse phase allowed for visualization of more extreme cycling during Phase 2 of the infection without affecting subsequent viral phases (Fig 8A, green dashed line). Increasing the virion production essentially eliminated the Phase 2 initial plateau resulting in earlier amplification (Fig 8B, green dashed line). Slower production in contrast lengthened the initial lower plateau Phase 2 and delayed subsequent viral phases (Fig 8B, red dotted line). Interestingly, combining a shorter cellular eclipse with a faster production cycle produces an almost single amplification phase analogous to that observed for many acute viral infections (Fig 8C, green dashed line) perhaps suggesting why such multiphasic viral infection kinetic patterns have not been universally observed when monitoring acute infection kinetics of other viruses. In contrast, combining a shorter cellular eclipse with a slower production cycle produces again the short eclipse extreme cycling this time during a longer Phase 2 followed by delay of all subsequent viral phases (Fig 8C, red dotted line). Combining a longer cellular eclipse with a faster production cycle resulted in an initial period of no viral production followed by immediate amplification (i.e., no Phase 2 initial plateau) with little effect on subsequent viral phases (Phases 3–6) (Fig 8C, green dashed line). While the longer cellular eclipse coupled with a slower production cycle resulted in an initial period of no viral production followed by delayed multiphasic viral amplification (Phases 2–6) (Fig 8D, red dotted line).

## Discussion

Standard population-based measurements of viral infection time courses typically show an initial eclipse phase followed by exponential increase ending either in cell lysis or steady state viral levels [13–21]. However, we recently reported a surprising complex HBV infection kinetics in chimeric uPA-SCID mice with humanized livers [9]. To investigate the dynamics underlying the unexpectedly complex HBV infection kinetics from inoculation to steady state in humanized uPA-SCID mice, we developed an ABM approach to explain the serum population kinetics from the perspective of individual cell infections. This allowed for the simulation of HBV production from individual cells as cycles rather than a continuous increase which

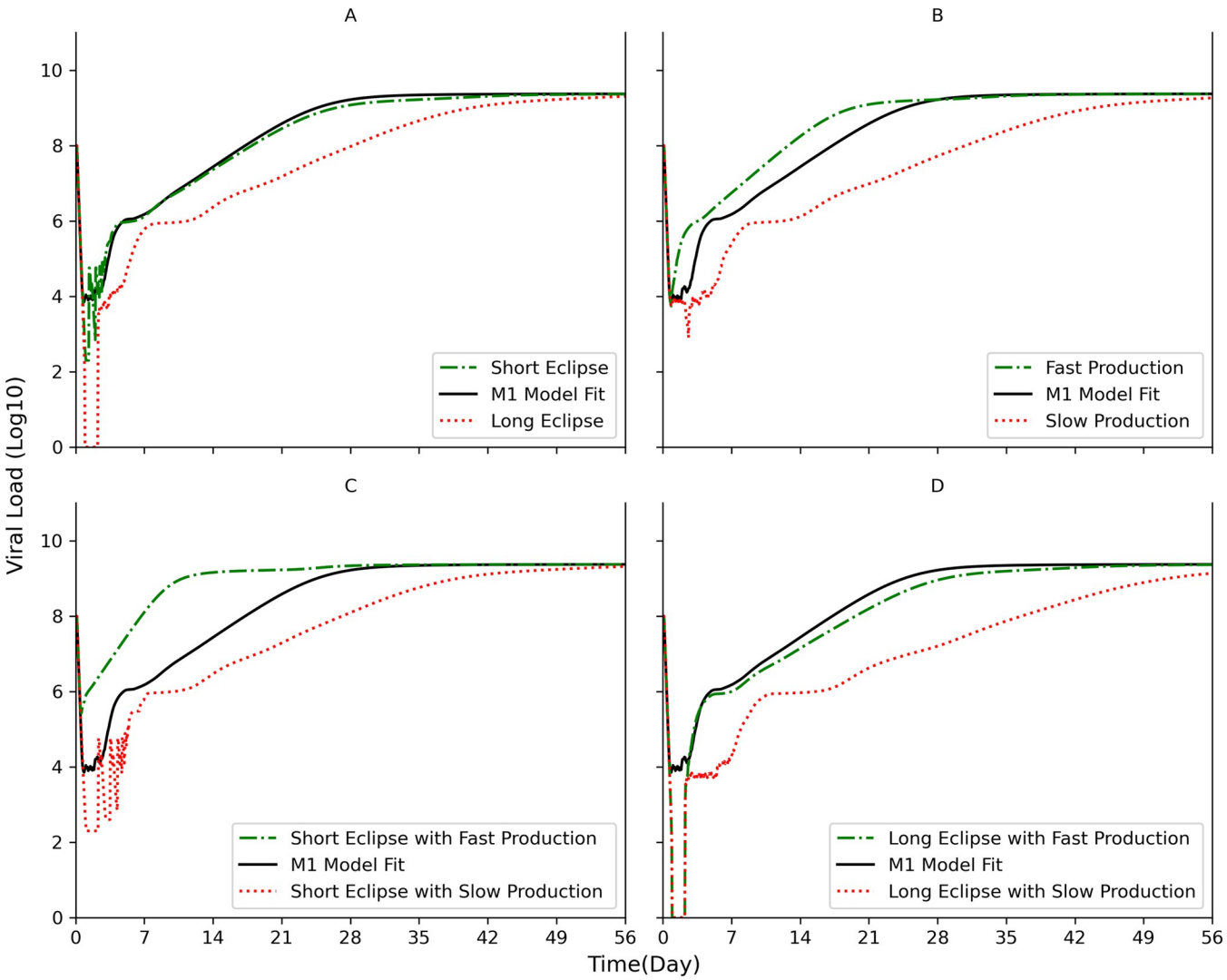


**Fig 8. Varying the eclipse phase length (Ω) and initial production cycle length ($\delta$).** Model simulations were run from time of inoculation until day 56 post inoculation (p.i.). Days 0–14 are shown here; days 0–56 are shown in Fig W in S1 Text. Parameters equal to that estimated for mouse 1 (M1) were used except for the indicated changes. **(A)** The parameter range of the eclipse phase was shortened to Ω = [0,5] hr (dashed green line) or extended to Ω = [36–72] hr (dotted red line). **(B)** The parameter range for the production cycle was reduced to $\delta$ = 1 hr (i.e., faster production, dashed green line) or increased to $\delta$ = 36 hr (i.e., slower production, dotted red line). **(C)** The short eclipse parameter range of Ω = [0,5] hr was combined with the fast (dashed green line) or slow (dotted red line) production parameter ranges used in (B). **(D)** same as **(C)** assuming extended eclipse phase to Ω = [36–72] hr. The model simulations for M1, Ω = [9,48] hr and to $\delta$ = 26 hr, is shown for comparison using solid black lines.

https://doi.org/10.1371/journal.pcbi.1011309.g008

resulted in the model accurately reproducing the multiphasic kinetic pattern observed and allowing for insights into the underlying viral dynamics.

The majority of mathematical models of acute viral infection are based on the assumption of well-mixed virus and cell populations [13–20]. For a noncytolytic virus such as HBV, in the absence of the development of immune response in which infected cells are targeted for loss/death at a faster rate compared to uninfected cells, these models predict a roughly monophasic viral increase that reaches a high viral load steady state (or peak) once all target cells are infected. Some models also accounted for an eclipse phase, e.g., [22,23], in which newly infected cells remain in a latent phase before becoming virion producing, but even with such additions a viral increase is predicted until all target cells are infected. For example, in the

chimpanzee model of acute hepatitis C virus (HCV) infection, viral levels increased in a biphasic manner with a transient viral decline in between (1 week p.i.) concomitantly with the induction of type I interferon [16]. However, HBV is often referred to as a stealth virus because it does not induce significant innate immune signaling [12], making immune signaling a less likely explanation for the shift from rapid expansion (Fig 1, Phase 3) to a slower interim plateau (Fig 1, Phase 4). While intrahepatic interferon induction cannot be ruled out without further experiments, we show here that this shift as well as all the phases observed can be accurately recapitulated by describing viral dynamics at the individual cell level combining the viral eclipse phase, the increasing rate of virus secretion based on increasing production cycles, and the resulting waves of new infection (Fig 6).

Viral kinetics early post-infection often exhibits a viral decline phase followed by lower plateau or undetectable viral level (a.k.a. eclipse phase) before exponential amplification. This is assumed to reflect the time period in which clearance of input virus in the blood is balanced by de novo viral production. We showed that mice inoculated with high ($10^8$) virus inoculation HBV DNA had a low viral plateau which lasted approximately 1–3 days p.i (Fig 1, Phase 2). Fitting the ABM with measured serum HBV DNA we estimated a range of 5 and 50 hours in which newly infected cells ($I_E$) cell remain in a latent phase before becoming virion producing infected cells ($I_P$). While this initially seemed like an unexpectedly broad parameter range, single cell analysis of viral infections has revealed analogously large ranges of variability in the progression of viral replication [24,25].

We previously reported [9] that HBV DNA inoculum size had no effect on initial HBV clearance (Fig 1, Phase 1), the viral doubling time during the HBV expansion phases (Fig 1, Phases 3 and 5), the length of the interim plateau (Fig 1, Phase 4), or viral steady-state levels (Fig 1, Phase 6), but rather resulted in a lower viral plateau (Phase 2) and a delay in detection of initial virus expansion (Fig 1, Phase 3), which subsequently delayed all other kinetic phases. Importantly, the model confirms this as simulating the infection kinetics in mice after HBV inoculation of $10^7$, $10^6$ or $10^4$ genome equivalents, requires no significant change in any of the estimated ABM parameters compared to the mice inoculated with $10^8$ genome equivalents except for the inoculation dose itself (Table 1), further supporting our ABM modeling approach.

Finding that the unusual multiphasic kinetics observed can be reproduced by a model that is based on the inherent cyclic nature of a viral lifecycle, raised the question why such complex kinetics were observed for HBV but not more broadly for other viral infections. While it is possible that such a multiphasic pattern could simply be missed in the absence of frequent sampling, this complex pattern was also eliminated by increasing viral production and reducing the eclipse phase in the model simulations (Fig 8C). Notably, these parameter changes are consistent with the faster lifecycles associate with many acute viruses and may explain why multiphasic viral kinetics has not been routinely observed for other viruses.

The current ABM does not account for intracellular HBV-host dynamics that explain the estimated timing of the viral production cycles but provides a prediction that can now be investigated. Our previous kinetic study [9], indicated that intrahepatic total HBV DNA, cccDNA, and RNA correlate with serum HBV DNA during infection in these mice. Thus, a future detailed intracellular kinetic analysis may shed light whether intrahepatic HBV RNA and/or DNA levels exhibit the same multiphasic amplification pattern and how cccDNA recycling impacts the level of HBV secretion early in infection.

Meanwhile, we show in the current study that the incorporation of viral production cycles into an ABM recapitulates the multiphasic serum HBV kinetic patterns observed in uPA-SCID mice reconstituted with humanized livers from inoculation to steady state [9]. Importantly, such complex HBV infection kinetics can be seen also in immunocompetent chimpanzees

[14,26] indicating that this complex picture is not unique to humanized uPA-SCID mice. Thus, using agent-based modeling to more accurate conceptualize virus production as cycles rather than a continuous increase allows us to reproduce the observed HBV infection dynamics in vivo and provides a new computational approach for simulating viral dynamics during acute infection.

## Materials and methods

### Ethics statement

All animal protocols from which the data in this manuscript were derived were performed in accordance with the Guide for the Care and Use of Laboratory Animals and approved by the Animal Welfare Committee of Phoenix Bio Co., Ltd (approval number 1031).

### Mice and HBV

The in vivo data investigated in silico herein has been previously published and described in detail in [9]. Briefly, humanized liver chimeric mice were produced by splenic injection of cryopreserved human hepatocytes into uPA/SCID mice as previously described [8,9]. Human hepatocyte repopulation rates were estimated by blood human albumin levels and chimeric mice showing repopulation rates of greater than 70% were injected with serum containing $10^4$, $10^6$, $10^7$ and $10^8$ copies HBV DNA (genotype C, Accession No. AB246345), originally provided by Dr. Sugiyama [27] via the tail vein. Preparation of the inoculum and methods utilized for DNA extraction and quantification of HBV DNA were performed as previously reported [9,28].

### Parameter estimations

We previously showed that during the first 6 h p.i., and 6–24 h p.i. HBV was cleared from blood with a $t_{1/2}$ of ~1 h and ~3 h, respectively, independent of inoculum size which ranged from $10^4$ to $10^8$ cp/ml [9]. Because the above two initial clearance phases have been combined into one, now jointly termed Phase 1 (Fig 1), we assumed a fixed clearance rate of virus from blood as $c = 0.5\ h^{-1}$. The fraction of virus in the blood (V) that was infectious was arbitrary set as $\rho = 0.5$. Based on the experimental data, HBV serum levels at steady state were set at, $V_{st}$ = 9.3±0.3. Viral production, $P_{st}$, is estimated at steady state where all target cells are infected ($I_p$ = $3\times10^8$ cells), which is equivalent to $P_{st} = \frac{0.5X10^{9.3\pm0.3}}{3X10^8} \approx$ between 2 and 7 virion/cell. The remaining parameters were estimated by calibrating the ABM with the experimental data (Table 1), using parameter constraints as shown in Table B in S1 Text that were obtained by preliminary ABM simulations and fitting with the experimental data using Anylogic.

### Model calibration

Model parameter fitting was done using a Genetic Algorithm (GA) [29,30] with the EMEWS framework [31] on the Midway2 high-performance computing (HPC) cluster at the University of Chicago. Midway2 has 400 nodes, each with 28 cores and 64GB of memory. Some additional development was done on the Bebop HPC cluster, managed by the Laboratory Computing Resource Center at Argonne National Laboratory. Bebop has 1024 nodes comprised of 672 Intel Broadwell processors with 36 cores per node and 128 GB of RAM and 372 Intel Knights Landing processors with 64 cores per node and 96 GB of RAM. The GA was implemented using the DEAP [32] evolutionary computation Python framework (specifically [33]: Chapter 7) and integrated into an EMEWS HPC workflow using EMEWS queues for Python (EQ/Py) [31]. The input parameters for the calibration were all in linear space. The objective function

used a log transform of the model outputs:

$$J = \sqrt{\frac{1}{n}\sum \frac{[log_{10}V(t_i) - log_{10}\hat{V}(t_i)]^2}{\sigma(t_i)^2}}, \quad (3)$$

where $log_{10}V(t_i)$ are the log-transformed predicted values of the viral load, $log_{10}\hat{V}(t_i)$ are the log-transformed experimental values, $\sigma(t_i)$ are the standard errors of the experimental data, which are assumed to be 0.5 for each data point $t_i$, and $n$ are the number of sample data points.

The use of HPC resources enable the concurrent evaluation of large numbers of design points (n = 102), reducing the time to solution. During each iteration of the GA, the best points from the currently evaluated population are selected using a tournament selection method to create a new population. Each of these points is then mated with another according to a cross-over probability and, finally, each of the resulting points is mutated according to a mutation probability. At each GA algorithm iteration, the new population is evaluated in parallel, and the evaluation results are gathered. The GA population size was set to 102, the mutation probability to 0.2, the crossover probability to 0.5, and the number of iterations to 25. On Midway2 the runtime for a typical run was 7.3 hours using full concurrency on 28 nodes (with 28 cores per node), or about 5700 core hours.

### Software

The agent-based model was developed on Anylogic V8.1.0 (an earlier version of the model was developed on Mason V17). The figures were plotted using Python (V3.8.8). The model fitting with empirical data was carried out using the EMEWS framework (https://emews.github.io/), DEAP library (V1.3) and Python (V3.8.5).

## Supporting information

**S1 Text. Tables A-B and Figs A-W.**
(DOCX)

## Acknowledgments

The research was completed with resources provided by the Research Computing Center at the University of Chicago (the Midway2 cluster), and the Laboratory Computing Resource Center at Argonne National Laboratory (the Bebop cluster).

## Author Contributions

**Conceptualization:** Atesmachew Hailegiorgis, Harel Dahari.

**Data curation:** Yuji Ishida, Michio Imamura, Nobuhiko Hiraga, Hiroshi Yokomichi, Chise Tateno, Kazuaki Chayama.

**Formal analysis:** Atesmachew Hailegiorgis.

**Funding acquisition:** Susan L. Uprichard, Kazuaki Chayama, Harel Dahari.

**Investigation:** Atesmachew Hailegiorgis, Vladimir Reinharz.

**Methodology:** Atesmachew Hailegiorgis, Nicholson Collier, Vladimir Reinharz, Danny Barash, Jonathan Ozik.

**Resources:** Yuji Ishida, Nicholson Collier, Hiroshi Yokomichi, Chise Tateno, Jonathan Ozik.

**Software:** Atesmachew Hailegiorgis, Nicholson Collier, Jonathan Ozik.

**Supervision:** Jonathan Ozik, Kazuaki Chayama, Harel Dahari.

**Validation:** Zhenzhen Shi.

**Visualization:** Atesmachew Hailegiorgis, Nicholson Collier, Zhenzhen Shi.

**Writing – original draft:** Atesmachew Hailegiorgis, Nicholson Collier, Zhenzhen Shi, Vladimir Reinharz, Masataka Tsuge, Jonathan Ozik, Susan L. Uprichard, Harel Dahari.

**Writing – review & editing:** Atesmachew Hailegiorgis, Yuji Ishida, Nicholson Collier, Michio Imamura, Zhenzhen Shi, Vladimir Reinharz, Masataka Tsuge, Danny Barash, Nobuhiko Hiraga, Hiroshi Yokomichi, Chise Tateno, Jonathan Ozik, Susan L. Uprichard, Kazuaki Chayama, Harel Dahari.

## References

1. WHO. Global hepatitis report, 2017 https://www.who.int/hepatitis/publications/global-hepatitis-report2017/en/. Accesed Oct 27,2020. [October 27,2020].
2. Revill PA, Chisari FV, Block JM, Dandri M, Gehring AJ, Guo H, et al. A global scientific strategy to cure hepatitis B. Lancet Gastroenterol Hepatol. 2019; 4(7):545–58. Epub 2019/04/15. https://doi.org/10.1016/S2468-1253(19)30119-0 PMID: 30981686; PubMed Central PMCID: PMC6732795.
3. Liu Y, Maya S, Ploss A. Animal Models of Hepatitis B Virus Infection-Success, Challenges, and Future Directions. Viruses. 2021; 13(5). Epub 2021/05/01. https://doi.org/10.3390/v13050777 PMID: 33924793; PubMed Central PMCID: PMC8146732.
4. Dandri M, Burda MR, Torok E, Pollok JM, Iwanska A, Sommer G, et al. Repopulation of mouse liver with human hepatocytes and in vivo infection with hepatitis B virus. Hepatology. 2001; 33(4):981–8. Epub 2001/04/03. https://doi.org/10.1053/jhep.2001.23314 PMID: 11283864.
5. Mercer DF, Schiller DE, Elliott JF, Douglas DN, Hao C, Rinfret A, et al. Hepatitis C virus replication in mice with chimeric human livers. Nat Med. 2001; 7(8):927–33. Epub 2001/08/02. https://doi.org/10.1038/90968 PMID: 11479625.
6. Rhim JA, Sandgren EP, Palmiter RD, Brinster RL. Complete reconstitution of mouse liver with xenogeneic hepatocytes. Proc Natl Acad Sci U S A. 1995; 92(11):4942–6. Epub 1995/05/23. https://doi.org/10.1073/pnas.92.11.4942 PMID: 7761429; PubMed Central PMCID: PMC41823.
7. Dandri M, Lutgehetmann M. Mouse models of hepatitis B and delta virus infection. Journal of immunological methods. 2014; 410:39–49. https://doi.org/10.1016/j.jim.2014.03.002 PMID: 24631647.
8. Tateno C, Yoshizane Y, Saito N, Kataoka M, Utoh R, Yamasaki C, et al. Near completely humanized liver in mice shows human-type metabolic responses to drugs. Am J Pathol. 2004; 165(3):901–12. https://doi.org/10.1016/S0002-9440(10)63352-4 PMID: 15331414; PubMed Central PMCID: PMC1618591.
9. Ishida Y, Chung TL, Imamura M, Hiraga N, Sen S, Yokomichi H, et al. Acute HBV infection in humanized chimeric mice has multiphasic viral kinetics. Hepatology. 2018; 68(2):473–84. https://doi.org/10.1002/hep.29891 PMID: 29572897.
10. Timm A, Yin J. Kinetics of virus production from single cells. Virology. 2012; 424(1):11–7. Epub 2012/01/10. https://doi.org/10.1016/j.virol.2011.12.005 PMID: 22222212; PubMed Central PMCID: PMC3268887.
11. Reinharz V, Ishida Y, Tsuge M, Durso-Cain K, Chung TL, Tateno C, et al. Understanding Hepatitis B Virus Dynamics and the Antiviral Effect of Interferon Alpha Treatment in Humanized Chimeric Mice. Journal of virology. 2021; 95(14):e0049220. Epub 2021/04/30. https://doi.org/10.1128/JVI.00492-20 PMID: 33910953; PubMed Central PMCID: PMC8223956.
12. Wieland SF, Chisari FV. Stealth and cunning: hepatitis B and hepatitis C viruses. Journal of virology. 2005; 79(15):9369–80. https://doi.org/10.1128/JVI.79.15.9369-9380.2005 PMID: 16014900; PubMed Central PMCID: PMC1181548.
13. Whalley SA, Murray JM, Brown D, Webster GJ, Emery VC, Dusheiko GM, et al. Kinetics of acute hepatitis B virus infection in humans. The Journal of experimental medicine. 2001; 193(7):847–54. https://doi.org/10.1084/jem.193.7.847 PMID: 11283157; PubMed Central PMCID: PMC2193367.
14. Murray JM, Wieland SF, Purcell RH, Chisari FV. Dynamics of hepatitis B virus clearance in chimpanzees. Proc Natl Acad Sci U S A. 2005; 102(49):17780–5. https://doi.org/10.1073/pnas.0508913102 PMID: 16306261.

15. Ciupe SM, Ribeiro RM, Nelson PW, Perelson AS. Modeling the mechanisms of acute hepatitis B virus infection. Journal of theoretical biology. 2007; 247(1):23–35. https://doi.org/10.1016/j.jtbi.2007.02.017 PMID: 17428501.

16. Dahari H, Major M, Zhang X, Mihalik K, Rice CM, Perelson AS, et al. Mathematical modeling of primary hepatitis C infection: noncytolytic clearance and early blockage of virion production. Gastroenterology. 2005; 128(4):1056–66. https://doi.org/10.1053/j.gastro.2005.01.049 PMID: 15825086.

17. Chertow DS, Shekhtman L, Lurie Y, Davey RT, Heller T, Dahari H. Modeling Challenges of Ebola Virus-Host Dynamics during Infection and Treatment. Viruses. 2020; 12(1). Epub 2020/01/23. https://doi.org/10.3390/v12010106 PMID: 31963118; PubMed Central PMCID: PMC7019702.

18. Burg D, Rong L, Neumann AU, Dahari H. Mathematical modeling of viral kinetics under immune control during primary HIV-1 infection. J Theor Biol. 2009; 259(4):751–9. Epub 2009/04/25. https://doi.org/10.1016/j.jtbi.2009.04.010 PMID: 19389409.

19. Zhang J, Lipton HL, Perelson AS, Dahari H. Modeling the acute and chronic phases of Theiler murine encephalomyelitis virus infection. Journal of virology. 2013; 87(7):4052–9. Epub 2013/02/01. https://doi.org/10.1128/JVI.03395-12 PMID: 23365440; PubMed Central PMCID: PMC3624189.

20. Boianelli A, Nguyen VK, Ebensen T, Schulze K, Wilk E, Sharma N, et al. Modeling Influenza Virus Infection: A Roadmap for Influenza Research. Viruses. 2015; 7(10):5274–304. Epub 2015/10/17. https://doi.org/10.3390/v7102875 PMID: 26473911; PubMed Central PMCID: PMC4632383.

21. Duke ER, Boshier FAT, Boeckh M, Schiffer JT, Cardozo-Ojeda EF. Mathematical Modeling of Within-Host, Untreated, Cytomegalovirus Infection Dynamics after Allogeneic Transplantation. Viruses. 2021; 13(11). Epub 2021/11/28. https://doi.org/10.3390/v13112292 PMID: 34835098; PubMed Central PMCID: PMC8618844.

22. Baccam P, Beauchemin C, Macken CA, Hayden FG, Perelson AS. Kinetics of influenza A virus infection in humans. Journal of virology. 2006; 80(15):7590–9. Epub 2006/07/15. https://doi.org/10.1128/JVI.01623-05 PMID: 16840338; PubMed Central PMCID: PMC1563736.

23. Madelain V, Oestereich L, Graw F, Nguyen TH, de Lamballerie X, Mentre F, et al. Ebola virus dynamics in mice treated with favipiravir. Antiviral Res. 2015; 123:70–7. Epub 2015/09/08. https://doi.org/10.1016/j.antiviral.2015.08.015 PMID: 26343011.

24. Schulte MB, Andino R. Single-cell analysis uncovers extensive biological noise in poliovirus replication. Journal of virology. 2014; 88(11):6205–12. Epub 2014/03/22. https://doi.org/10.1128/JVI.03539-13 PMID: 24648454; PubMed Central PMCID: PMC4093869.

25. Guo F, Li S, Caglar MU, Mao Z, Liu W, Woodman A, et al. Single-Cell Virology: On-Chip Investigation of Viral Infection Dynamics. Cell Rep. 2017; 21(6):1692–704. Epub 2017/11/09. https://doi.org/10.1016/j.celrep.2017.10.051 PMID: 29117571; PubMed Central PMCID: PMC5689460.

26. Asabe S, Wieland SF, Chattopadhyay PK, Roederer M, Engle RE, Purcell RH, et al. The size of the viral inoculum contributes to the outcome of hepatitis B virus infection. Journal of virology. 2009; 83(19):9652–62. https://doi.org/10.1128/JVI.00867-09 PMID: 19625407; PubMed Central PMCID: PMC2748002.

27. Sugiyama M, Tanaka Y, Kato T, Orito E, Ito K, Acharya SK, et al. Influence of hepatitis B virus genotypes on the intra- and extracellular expression of viral DNA and antigens. Hepatology. 2006; 44(4):915–24. https://doi.org/10.1002/hep.21345 PMID: 17006908.

28. Abe A, Inoue K, Tanaka T, Kato J, Kajiyama N, Kawaguchi R, et al. Quantitation of hepatitis B virus genomic DNA by real-time detection PCR. Journal of clinical microbiology. 1999; 37(9):2899–903. https://doi.org/10.1128/JCM.37.9.2899-2903.1999 PMID: 10449472; PubMed Central PMCID: PMC85408.

29. Holland JH. Adaptation in Natural and Artificial Systems: An Introductory Analysis with Applications to Biology, Control, and Artificial Intelligence: A Bradford Book, Cambridge, Mass.; 1992.

30. Goldberg DE. Genetic algorithms in search, optimization, and machine learning. Reading, Mass.: Addison-Wesley Pub. Co.; 1989. xiii, 412 p. p.

31. Ozik J, Collier N, Wozniak J, Spagnuolo C, editors. From Desktop to Large-Scale Model Exploration with Swift/T. Winter Simulation Conference Proceedings; 2016; Washington, D.C. https://doi.org/10.1109/WSC.2016.7822090 PMID: 31239603

32. Félix-Antoine F, De Rainville FM, Gardner MA, Parizeau M, Gagné C. DEAP: Evolutionary Algorithms Made Easy. Journal of Machine Learning Research 2012; 13:2171–5.

33. Back T, Fogel DB, Michalewicz T. Evolutionary computation. Bristol, Philadelphia: Institute of Physics Publishing; 2000.